

# A simulation study of the digital ion trap mass spectrometer

Li Ding\*, Michael Sudakov, Sumio Kumashiro

*Shimadzu Research Laboratory (Europe) Ltd., Wharfside, Trafford Wharf Road, Manchester M17 1GP, UK*

Received 8 March 2002; accepted 21 August 2002

## Abstract

The theoretical foundation for the digital ion trap (DIT) is presented in outline where the study of ion motion in the DIT employed the  $a$ ,  $q$ ,  $\beta$  parameter framework of conventional ion trap study. A user program for SIMION has been developed to simulate the DIT operation in real environment allowing the higher-order fields to be represented. Three-dimensional random ion buffer gas collisions were modelled where Maxwellian velocity distribution of the buffer gas was considered. A mass-selective ejection scan method is described and simulated, where both the trapping quadrupole field and dipole excitation field are driven digitally and their frequencies are scanned proportionally. The performances of the stretched ion trap and a new field-modified ion trap are simulated and compared. Using a field-adjusting electrode near the end-cap aperture, the new ion trap is able to achieve higher mass resolution for both forward and reverse mass scans. The simulation studies also the relation between the ejection time and the parameters of digital dipole excitation, the influence of space charge, duty cycle modulation as an alternative ejection scan method, and ion introduction into the ion trap. (Int J Mass Spectrom, in press)

© 2002 Published by Elsevier Science B.V.

**Keywords:** Digital ion trap; Simulation; Ion neutral collision; Resonance ejection; Higher-order field

## 1. Introduction

The quadrupole mass filter and the quadrupole ion trap analyser have been widely used for mass analysis since their invention by Paul and Steinwedel [1]. With the introduction of the mass-selective instability mode and the resonance ejection technique [3–5], the performance of the ion trap mass spectrometer was enhanced greatly. The mass range was extended to allow the analysis of large biomolecular ions, and the MS–MS mode provides the opportunity to elucidate the structure of these complex molecules.

To date, most studies of the quadrupole ion trap have been based on the solution of the Mathieu equa-

tion which describes the ion motion in a quadrupole electric field driven by a sinusoidal wave voltage generated by an rf generator. The analogue rf generator comprises a driving electric circuit and a resonating network, which includes the quadrupole device as a load. The output waveform and frequency are thus fixed in order to keep the circuit resonant. Mass scans can only be achieved by changing the rf voltage amplitude, or sometimes with a proportional dc voltage component. Analysis of high mass requires an rf voltage of some tens of kilovolts which might cause a discharge problem.

The use of a frequency scan rather than a voltage scan was reported for both a quadrupole mass filter [6] and for high mass analysis with a MALDI ion trap mass spectrometer [7]. Waveform genera-

\* Corresponding author. E-mail: li.ding@srlab.co.uk

tors and power amplifiers were used to provide the variable frequency sine wave voltage. However, it is not necessary to use a sinusoidal waveform to drive a quadrupole field for ion trapping and selection. In the 1970s, Sheretov and Terent'ev [8] studied the pulse-fed hyperboloid mass analyser and derived the conditions of ion trajectory stability. Mass analysis with a mass filter and an ion trap driven by rectangular waveform voltages were reported by Sheretov et al. [9] and Richards et al. [10]. Recently, the ion motion driven by a rectangular wave quadrupole field has also been studied with the conventional  $a$ - $q$  parameters system and the frequency of secular motion of ions has been derived using a pseudo-potential approximation [11]. An MS experiment using both digital driving and digital dipole excitation for resonance ejection of ions was reported [12]. The ion trajectory stability in a quadrupole field with various periodic waveforms has also been studied [13]. All these research activities suggested the possibility of exploiting the digital operation of quadrupole ion trap mass spectrometers.

In a digital ion trap (DIT) mass spectrometer, the trapping electric field, and possibly also the excitation electric field, are provided by switching voltages. The timings of these switching circuits are controlled by high precision digital circuits, which precisely control the frequency and modulation of the digital waveform. It is normally the frequency, rather than the amplitude of the driving voltage, that is scanned during a mass scan. Compared with an rf frequency scan through an amplifier, the digital method offers higher energy consumption efficiency as its circuit works in switching mode. Compared with the conventional rf resonator method, the DIT not only has a wider range of mass scan, as a result of the frequency scan, but also provides more flexibility of operation. The driving voltage in the DIT can be started and cut-off instantly facilitating pulsed ion introduction and ejection without a complicated design for the rf generator [14]. The digital waveform can also be tailored by software to implement specific manipulation of the ions. One of the examples is to achieve parametric resonance as described later and use the parametric resonance

for modification of the stability diagram and cause a quadrupolar excitation [13].

While many potential applications can be foreseen, however, the investigation of the DIT is still in its infancy. The theoretical treatment of the DIT is of little value to the practical work because of the complexity of the real trapping field in the ion trap where higher-order multipole fields may be introduced unavoidably or deliberately. We believe that only a simulation of ion motion in a practical ion trap geometry can reveal the real features of the DIT.

In a study of the analogue rf voltage driven ion trap mass spectrometer, Julian et al. [15] simulated multi-ion motion in an ion trap using the software program ITSIM. Although the work referred to a stretched ion trap, it did not consider the multipole field effect, which is one of most important factors affecting ion trap performance. The ITSIM program used only a one-dimensional collision model and the paper did not show any result related to space charge effects since the number of ions in the simulation was low.

In this paper, we review the fundamental principles of DIT operation and present our simulation study of the DIT mass spectrometer using SIMION 7 software combined with our own user programs including a three-dimensional Monte Carlo collision module.

## 2. The theoretical basis

The fundamental theory of operation of quadrupole devices driven by a rectangular or pulsed wave voltage has been described elsewhere [8,11,13]. Here, we summarise those basic points that relate to the DIT operation and present them in a framework similar to that used conventionally for the study of the sinusoidal wave ion trap.

### 2.1. Stability of trajectories

In the steady trapping operation, a periodic rectangular wave voltage generated by switching between a high voltage level  $V_1$  and a low voltage level  $V_2$  is applied to the ring electrode of the ion trap. This

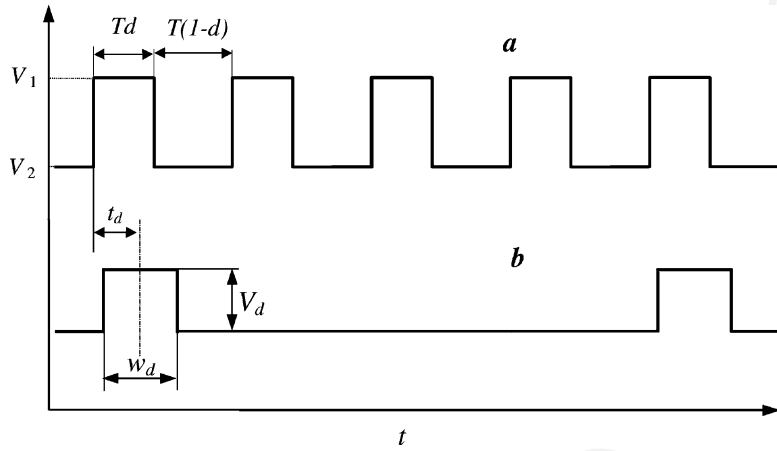


Fig. 1. The digital waveforms used for operating a DIT. (a) The drive voltage on the ring electrode. (b) The excitation voltage applied to the end-cap electrodes. The voltages are scaled arbitrarily.

periodic waveform is shown in Fig. 1. In this situation, the Mathieu equation is no longer applicable for the prediction of ion motion, so the matrix transform method [13,16] must be used. The Mathieu parameters  $a$ ,  $q$ , however, are still useful for the presentation of ion trajectory stability.

In every time period  $T$ , the transfer of an ion's coordinates in phase space can be expressed as

$$\begin{pmatrix} u_{n+1} \\ \dot{u}_{n+1} \end{pmatrix} = \Omega \begin{pmatrix} u_n \\ \dot{u}_n \end{pmatrix} \quad (1)$$

where the coordinate  $u = z$  for the following discussion:  $\dot{u} = (2/\Omega)(dz/dt)$ ,  $\Omega = 2\pi/T$ , and the transfer matrix

$$\Phi = \begin{pmatrix} \phi_{11} & \phi_{12} \\ \phi_{21} & \phi_{22} \end{pmatrix}$$

is the product of the transfer matrices  $\Phi_1$  and  $\Phi_2$ , for the high level excursion  $Td$  and the low level excursion  $T(1-d)$ , respectively. Here,  $d$  is the duty cycle of the waveform. In order to link the transfer matrix to the conventional Mathieu parameters:

$$a_z = -\frac{8eU}{m\Omega^2 r_0^2} \quad (2a)$$

and

$$q_z = \frac{4eV}{m\Omega^2 r_0^2} \quad (2b)$$

we take the  $U$  and  $V$  in the above definition to be the average values of the dc and ac components of the rectangular wave voltage applied to the ring electrode. These average values are:

$$U = dV_1 + (1-d)V_2 \quad (3a)$$

$$V = 2(V_1 - V_2)(1-d)d \quad (3b)$$

Deriving from Newton's equation, we obtain:

$$\phi_{11} = \frac{\text{ch}(K_1\pi d) \text{ch}[K_2\pi(1-d)] + \text{sh}(K_1\pi d) \text{sh}[K_2\pi(1-d)]K_2}{K_1} \quad (4a)$$

$$\phi_{12} = \frac{\text{ch}(K_1\pi d) \text{sh}[K_2\pi(1-d)]}{K_2} + \frac{\text{sh}(K_1\pi d) \text{ch}[K_2\pi(1-d)]}{K_1} \quad (4b)$$

$$\phi_{21} = \text{sh}(K_1\pi d) \text{ch}[K_2\pi(1-d)]K_1 + \text{ch}(K_1\pi d) \text{sh}[K_2\pi(1-d)]K_2 \quad (4c)$$

$$\phi_{22} = \frac{\text{sh}(K_1\pi d) \text{sh}[K_2\pi(1-d)]K_1}{K_2 + \text{ch}(K_1\pi d) \text{ch}[K_2\pi(1-d)]} \quad (4d)$$

where

$$K_1 = \sqrt{\frac{q_z}{d} - a_z} \quad (5a)$$

and

$$K_2 = \sqrt{\frac{q_z}{d-1}} - a_z \quad (5b)$$

Here, the hyperbolic functions may change to sin and cos when  $K_1$ ,  $K_2$  become imaginary. The condition for a stable transfer matrix is that the eigenvalues of the transfer matrix in (1) have a modulus equal to unity. From this condition we can obtain the stability diagram for rectangular wave driving. A stability diagram in conventional  $a$ - $q$  coordinates is plotted in Fig. 2 with duty cycle  $d$  as an additional parameter for the motion in axial direction. An ion trajectory will be stable if motions in both the axial and radial

directions are stable. (A part of the combined stability diagram can be seen in Fig. 10, which is prepared for later discussion.)

For the case of a square wave, where  $d = 0.5$ , the  $\beta_z = 1$  boundary of the first stability region has a relatively smaller  $q_z$  value than in the case of sinusoidal waveform and crosses the  $q_z$  axis at 0.712.

## 2.2. Secular motion in the DIT

It can be further proved that

$$\phi_{11}\phi_{22} - \phi_{12}\phi_{21} = 1 \quad (6)$$

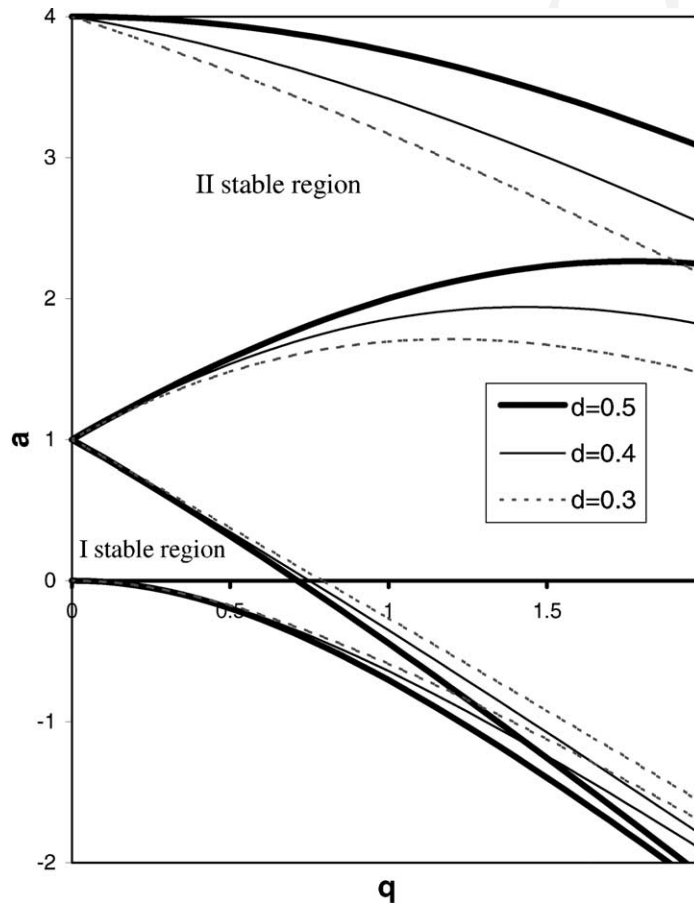


Fig. 2. The stability diagram for an ion trap driven by digital waveforms having a duty cycle  $d$  at 0.3, 0.4 and 0.5. The diagram shows the first and second stable regions in either  $z$  or  $r$  direction, and uses the same definition for  $a$  and  $q$  parameters as in the conventional harmonic rf driven ion trap.

By using (1) for the two sequential rectangular wave cycles and from consideration of Eq. (6), we obtain:

$$z_{n+1} + z_{n-1} = (\phi_{11} + \phi_{22})z_n \quad (7)$$

The following solutions satisfy Eq. (7) at the end of every drive rectangular wave cycle on a stable ion trajectory:

$$z_n = A_l \cos n(2l \pm \beta_z)\pi + B_l \sin n(2l \pm \beta_z)\pi \quad (8)$$

where  $l = 0, 1, 2, 3, \dots$ , and  $\beta_z$  should satisfy  $\cos \beta_z \pi = (\phi_{11} + \phi_{22})/2 < 1$ . Therefore, the ion motion is the composite of harmonic oscillations at the frequencies of

$$\omega_{z,l} = \frac{(2l \pm \beta_z)\pi}{T} = \left(l \pm \frac{1}{2}\beta_z\right) \Omega \quad (9)$$

For  $l = 0$ , the fundamental frequency component has the same form as the so-called secular motion frequency. Thus, we have unified the concept of secular motion which is widely used in the analysis of solutions of the Mathieu equation and the concept of ‘characteristic trajectory’ introduced by Sheretov and Terent’ev [8]. The secular frequency for the DIT can be expressed then as

$$\omega_z = \frac{\Omega}{2\pi} \arccos \frac{\phi_{11} + \phi_{22}}{2} \quad (10)$$

The oscillation at this frequency is caused by the integrated effect of the rectangular wave electric field and its frequency is a function of ion mass/charge ratio and the repetition rate of the driving rectangular wave. Each  $\beta_z$  value corresponds to a frequency of secular motion and  $\beta_z = 0$  and 1 corresponds to the stability boundaries. As in the sinusoidal waveform driven quadrupole field, the secular motion can be stimulated by various methods such as dipolar excitation and quadrupolar excitation in order to achieve different kinds of performance for mass analysis.

During a scan of resonant ejection in the DIT, it is preferable to apply a digital waveform to the end-cap electrodes for excitation of the secular motion of ions. The digital waveform is preferably a rectangular pulse

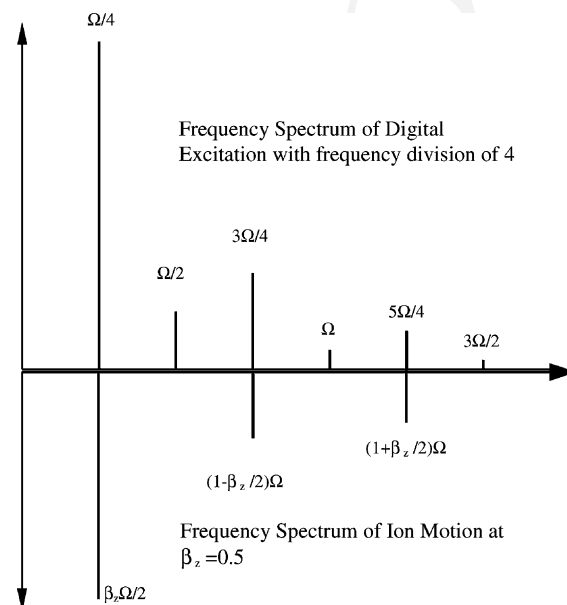


Fig. 3. Frequency components of a digital excitation signal with the frequency  $\omega_{ex} = \Omega/4$  and the frequency components of corresponding ion motion, scaled relative to the drive rectangular wave frequency  $\Omega$ .

signal (also displayed in Fig. 1) with a repetition rate of a fraction of the driving digital waveform. Fig. 3 shows the frequency components of the digital excitation signal having a frequency equal to 1/4 of that of the drive voltage. In such a case not only is the fundamental frequency component  $\omega_0$  of the excitation waveform used to excite the ion's secular motion, but some higher harmonic components may also match the other higher-order components (say  $\Omega(1 - \beta_z/2)$ ) of the ion motion of the same  $q_z$  value. None of these components will induce resonance excitation in ions having a different  $q_z$  value. For an excitation pulse rate corresponding to a small  $\beta_z$  value, the higher harmonic component may be effective in exciting other trapped ions within the first stability region. In order to avoid this, the digital waveform can be tailored to cancel the second and/or the third harmonic components. A pure square wave is just an example of waveform having no second harmonic component.

### 3. Simulation program

Mass analysis with the DIT is a complex series of operations involving the ions. The ion trajectory simulation of these operations should have following capabilities:

1. to allow a time-varying electric field;
2. to model the collision between a gaseous ion and a buffer gas molecule or atom by three-dimensional scattering;
3. to include a higher-order multipole field and field distortion near the entrance and exit apertures; and
4. to take into account the space charge effects when many ions are trapped simultaneously and flying together.

Our simulation work has been based on the SIMION 7 software for which we developed our own user programs. Advances in computing speed and memory size of a PC have enabled us to make a user program that encompasses the above requirements. In this work, a 1.6 GHz and a 800 MHz PCs were employed for different parts of the simulations.

The model ion traps are about the same size as the commercial one where the ring electrode is of i.d. 20 mm. In order to estimate the errors of coarseness of the potential grid, grid units of 0.025, 0.05, and 0.1 mm were tested. Only minor changes ( $\sim 0.1\%$  for  $\omega_z$ ) were resulted in by changing grid size from 0.05 to 0.025 mm. A coarser potential grid (0.1 mm/gu) will create an obvious error in the simulation involving area near the end-cap hole, because the number of the grid points representing the area is too small. All results in this paper were obtained using a grid unit size of 0.05 mm for the ion trap area.

The time step was fixed at  $T/200$  for most of the simulations and SIMION's time step adjustment was disabled. We have found that the simulation only gave accurate results when the time step for ion flight was an integral division of  $T$ , the period of the digital drive voltage.

All of the simulations discussed in this paper used a  $\pm 1$  kV square wave drive voltage unless otherwise specified. Mass scanning was achieved by increasing

or decreasing of the frequency in a way that a fixed amount of increment of period  $\Delta T$  is add to the current period  $T$  after the output of every  $N$  periods of the waveform. When the ion trap has standard geometry with  $r_0 = 10$  mm and the resonance ejection occurs at  $q_z = \beta_z = 0.5$  (dc-free square wave), from Eq. (2b) the mass/charge ratio of the ejecting ion has the following relationship with the period of the drive waveform:

$$\frac{m}{Z} = 195.5T^2(\text{Th}) \quad (\text{with } T \text{ in } \mu\text{s}) \quad (11)$$

When the number of repetitions  $N$ , between the increments of period, is fixed, we obtained the scan speed as

$$\frac{\Delta(m/Z)}{\Delta t} = 391 \times 10^6 \frac{\Delta T}{N} \quad (12)$$

In this way, a linear mass scan is achieved although the frequency has a non-linear relationship with the time. The scan speed given by Eq. (12) is important for comparing the performance between different traps and scan modes.

The software for the collisional cooling simulation, is included in an example of the user program in the standard package of SIMION 7, but it does not reflect the true pattern of ion motion [17]. This model causes the ion velocity decrease continuously resulting in zero cloud size after sufficient time. In our user program, the true three-dimensional collisions were modelled and the Maxwellian energy distribution of the buffer particles has also been taken into account.

In each computation step of our simulations, we calculate the probability of a collision between the ion and a buffer particle by the following equation:

$$P = 1 - \exp\left(-\frac{D}{\lambda}\right), \quad D = v_{\text{rel}} \Delta t, \quad \lambda = \frac{1}{n\sigma} \quad (13)$$

Here  $D$  is the distance of ion flight during one computation step  $\Delta t$ ,  $\lambda$  the mean free path,  $n$  the number density of the buffer particles,  $\sigma$  the collision cross-section. The important point of Eq. (13) is the use of the relative ion velocity  $v_{\text{rel}}$  for calculating an ion's flight distance between collisions. The relative



velocity between a flying ion and a buffer particle is obtained by averaging the ion velocity with respect to all possible velocities of the buffer particles:

$$v_{\text{rel}} = \iiint |\vec{v}_{\text{ion}} - \vec{v}| \left( \frac{m_b}{2\pi kT_b} \right)^{3/2} \times \exp \left( -\frac{m_b \vec{v}^2}{2kT_b} \right) dv_x dv_y dv_z \quad (14)$$

where  $m_b$  and  $\vec{v}$  are the buffer particle mass and velocity, respectively. The buffer velocity distribution is Maxwellian with an absolute temperature of  $T_b$ , and  $k$  is Boltzmann's constant. Evaluation of Eq. (14) gives the following:

$$v_{\text{rel}} = v_0 \left[ \left( s + \frac{1}{2s} \right) \int_0^s \exp(-x^2) dx + \frac{1}{2} \exp(-s^2) \right],$$

$$s = \frac{v_{\text{ion}}}{v_T}, \quad v_0 = \sqrt{\frac{8kT_b}{\pi m_b}}, \quad v_T = \sqrt{\frac{2kT_b}{m_b}} \quad (15)$$

The variation of  $v_{\text{rel}}$  with  $v_{\text{ion}}$  is presented in Fig. 4 for the case of He buffer gas at room temperature. It

is important to take into account this dependence in ion trap simulations, because the ion may have considerably different velocity in different operation stages. When the ion is injected into the trap, or ion motion is excited, the kinetic energy of ion is much greater than that of the buffer gas atoms. The ion's absolute velocity, in this case, may also be much greater than the average velocity of the buffer atoms, so the relative velocity is almost equal to the ion velocity. When the ion cloud comes into equilibrium with the buffer gas, the kinetic energy of an ion is of the same order as the average kinetic energy of buffer particles. For high mass ions, the equilibrium ion velocity is much smaller than the average velocity of the buffer molecules. According to Fig. 4, the relative velocity of the ion in this case is almost equal to the average buffer atom velocity,  $v_0$ . Hence, in the simulation of ion trap operation, the collision probability should relate to the relative velocity rather than ion velocity or buffer particle velocity alone.

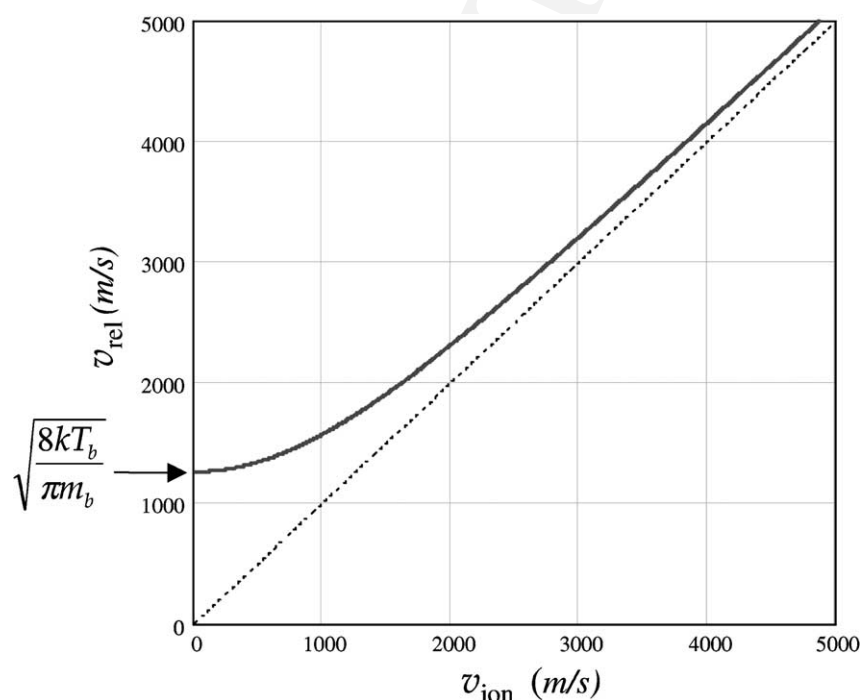


Fig. 4. The relative velocity used for calculation of ion buffer gas collision probability vs. the velocity of ion motion. The buffer gas is helium with temperature at 300 K.

The resultant probability from Eq. (13) is then compared with a random number  $0 < \xi < 1$ . When the random number is smaller than the probability then we assume that a collision has happened. A real three-dimensional statistical simulation is carried out in following steps:

1. loading the vector of ion's velocity  $\vec{v}_{\text{ion}}$  from SIMION before collision;
2. generating a random vector of buffer particle velocity assuming they obey Maxwellian distribution;
3. randomly choosing the projecting point of the buffer particle at the ion surface so the angles of collision can be calculated according with the hard sphere model;
4. calculating the velocity of the ion after the collision explicitly in accordance with energy and momentum conservation.

With such a real three-dimensional random collision module embedded in the user program, various kinds of ion buffer gas interaction can be demonstrated with a fixed or variable drive voltage. When the ion velocity is well over the buffer gas velocity, then the model shows that the rate of ion energy loss is proportional to the square of the ion's velocity (square damping). When the ion velocity is small, the rate of energy loss becomes proportional to the ion velocity (linear damping). This behaviour was previously studied in theory [18] but is demonstrated here for the first time in an ion trap simulation. When the ion initial velocity is so small that its kinetic energy is below the thermal kinetic energy of the buffer gas, the ion may be heated up. In all cases, the ions will finally reach an equilibrium with the buffer gas and will form an ion cloud in the centre of the ion trap with a certain fluctuation in size.

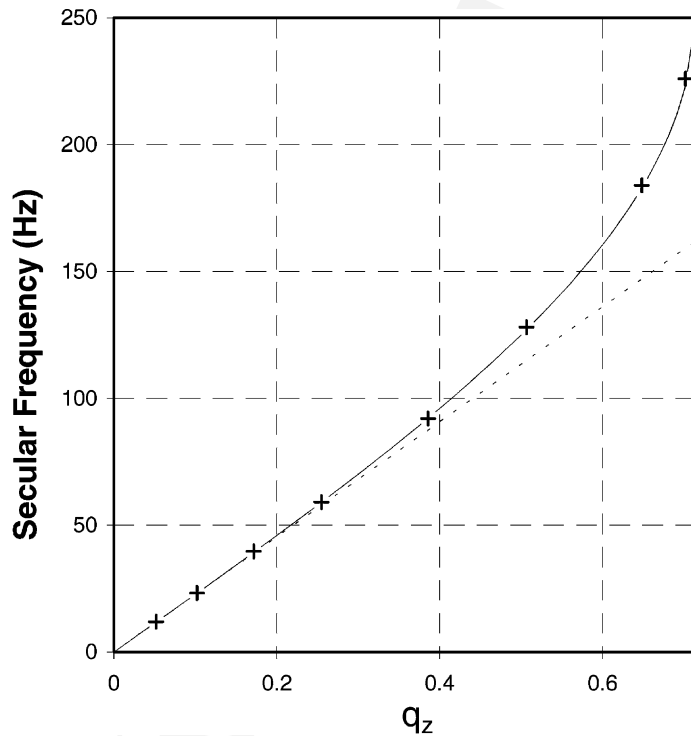


Fig. 5. Secular frequency predicted with Eq. (10) (solid line), with pseudo-potential approximation in [11] (dashed line) and measured from simulation (+ symbols);  $\Omega = 500$  kHz.



## 4. Simulation results and discussions

### 4.1. Secular motion

Ion motion in the ion trap was observed and the secular frequency  $\omega_z$  was measured during ion flight by recording the time that ion pass the  $z = 0$  plane (for spatial orientation, refer to Fig. 8) and calculating the mean value of the repetition period. For a square wave driving voltage (duty cycle 0.5), the measured secular frequency is illustrated in Fig. 5 in comparison with those predicted by theories. The measured  $\omega_z$  agrees very well with the value obtained from Eq. (10) over all of the stable  $q_z$  range while the pseudo-potential approximation only matches the simulation results in the low  $q_z$  area. It should be noted that the measured  $\omega_z$  value depends on the amplitude of ion oscillation due to the higher-order field, which exists in the real ion trap. When the trajectory of an ion reaches the vicinity of the end-cap holes,  $\omega_z$  decreases. However, the situation might be different when an additional dc field

is placed around the end-cap hole by an external electrode. This phenomenon will be further discussed later.

### 4.2. Resonance ejection scan

For a forward mass scan, the frequency of the driving rectangular wave, as well as the dipolar excitation frequency, was swept down, and for a reverse scan, both frequencies were swept up. In each simulation, the evolution of the ion's oscillation amplitude was studied using a plot of the return points at one side of the ion trap (where  $z > 0$ , and we expect ions are ejected through this side). The graph of return points gives a lot of information about the secular oscillation. Fig. 6 shows such a graph for the moment just before ejection through the end-cap hole at  $\beta_z = 0.5$ . To make it clearer, part of ion trajectory is also plotted using the dashed dot line. The minor ticks on the time axis shows the driving rectangular wave period and the space between vertical grids is roughly the secular motion period ( $\sim 4T$ ). The points on the branches A

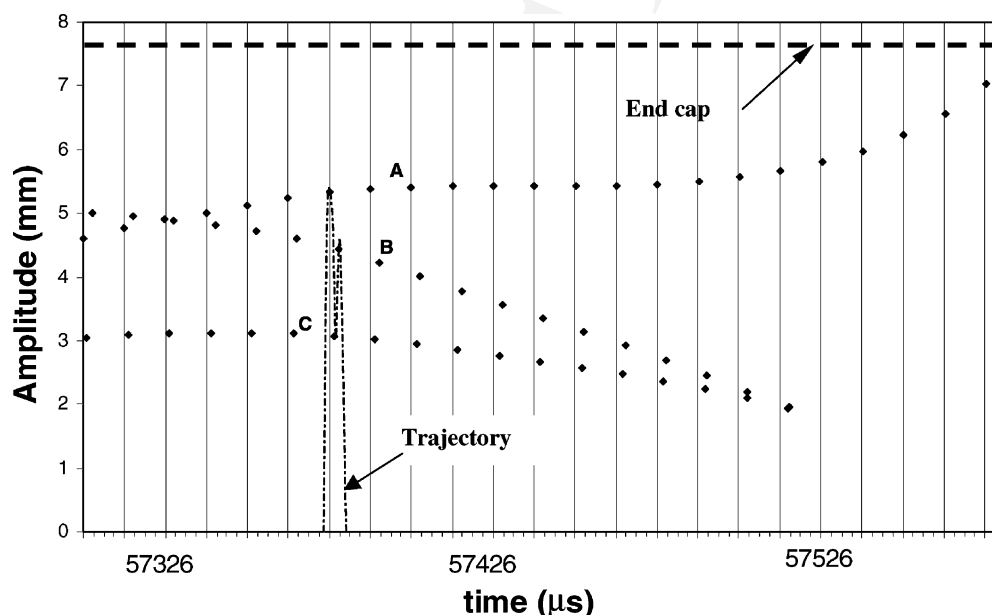


Fig. 6. A record of the returning point on the  $z > 0$  side of the ion trap. Rectangular drive voltage  $\pm 1000$  V, dipolar excitation at  $q_z = 0.5$ ,  $V_{\text{dip}} = 50$  V, width  $0.2T$ ,  $m = 3500$  Da, charge number  $Z = 2$ , buffer gas He pressure  $1 \times 10^{-3}$  mbar at 300 K. Dot series A and B represent the two local maxima and C the local minimum of the trajectory, a portion of which is shown by using a dashed dotted curve. Also shown in the figure is the position of the end-cap for the stretched ion trap.

and B represent the  $z_{\max}$  and those on the branch C represent the  $z_{\min}$ , all being the return points of the ion trajectory. These return points are always in the middle of negative (A and B) or positive (C) excursion of the rectangular wave drive voltage, so they roughly mark the phase of the drive rectangular wave. At a time of 57,326  $\mu\text{s}$ , one can see two equal maxima on  $z > 0$  side, but later the first one (A branch) prevails over the second one (B branch). This evolution indicates that the secular frequency is shifting above the  $\Omega/4$  point at which we assigned the ejection. This is not only a results of the scan by which  $q_z$  is continuously increased, but also a result of a secular frequency shift caused by the higher-order field. Through such a detailed study we can gain better understanding of ion motion in the presence of an imperfect field.

In the following section, only the biggest  $z_{\max}$  was plotted in order to show the full amplitude.

#### 4.3. With a stretched trap

Simulation of ion motion in a 10% stretched ion trap showed that the secular frequency continually increases with increase of the ion's oscillation amplitude. This is apparently a result of higher-order multipole fields involved with such an electrode structure. Fig. 7a shows the amplitude evolution during a forward resonance ejection scan for a 10% axially stretched ion trap. Several features can be observed in this evolution. First, a relative large dipolar excitation voltage (here a 50 V, 20%  $T$  pulsed waveform is used) is needed for the ejection of ions. When the intensity of dipolar excitation is not sufficient, the ion trajectory may start to expand at resonance but then lose the resonance condition when the amplitude gets bigger and a contraction follows. This is similar to the phenomenon which exists in an analogue drive situation and has been discussed by Franzen et al. [19].

Second, once the intensity of dipolar excitation is sufficient, the final trajectory expansion where an ion is ejected from the ion trap occurs very rapidly. During the simulation, we can colour mark the trajectory to indicate when the pulsed dipolar voltage is on duty. We can see clearly a positive feed-back in the

forward ejection: closer to resonance  $\rightarrow$  an amplitude increase  $\rightarrow$  an increase in secular frequency  $\rightarrow$  match of the resonance  $\rightarrow$  amplitude increase abruptly. The ion does not hesitate at the end-cap hole during the ejection, therefore no or small chemical shift [20] is linked to such an ion trap when it is used for a forward scan.

Third, the required high intensity excitation voltage induces a high beat as the ion motion progresses in time. The time that an ion enters the final 'positive feed-back' ejection depends on the phase of the beat which is randomised by collisions with the buffer gas. Although the ejection is fast, it is still difficult to get high resolution unless the scan speed is extremely slow.

When using a stretched ion trap for a reverse mass scan, the feed-back effect becomes negative so the expansion of the ion trajectory is extremely slow. Fig. 7b shows the evolution of ion trajectory amplitude during a reverse scan with the same scan speed as in Fig. 7a. Ion ejection suffers a great delay and poor mass resolution is observed.

#### 4.4. With a field adjustable trap

Recent studies [20] have shown that the end-cap apertures, where ions enter and are ejected from the ion trap, provide the primary defect to the quadrupole field. This defect causes the chemical shift and delay of ejection that contributes to poor resolution of a mass scan. The addition of a higher-order multipole field, by stretching the ion trap in the axial direction, can be employed to avoid this deleterious influence and improve the analytical performance. The above simulation results showed that the same scenario applies also to the DIT. However, our simulation has also found many shortcoming of the stretched geometry. We believe that, by reducing the defect of the field around the end-cap apertures, high mass resolution can also be achieved without a significant higher-order multipole field.

Simulations were carried out on a new type of the quadrupole ion trap where an external field-adjusting electrode was used to compensate for the defect of

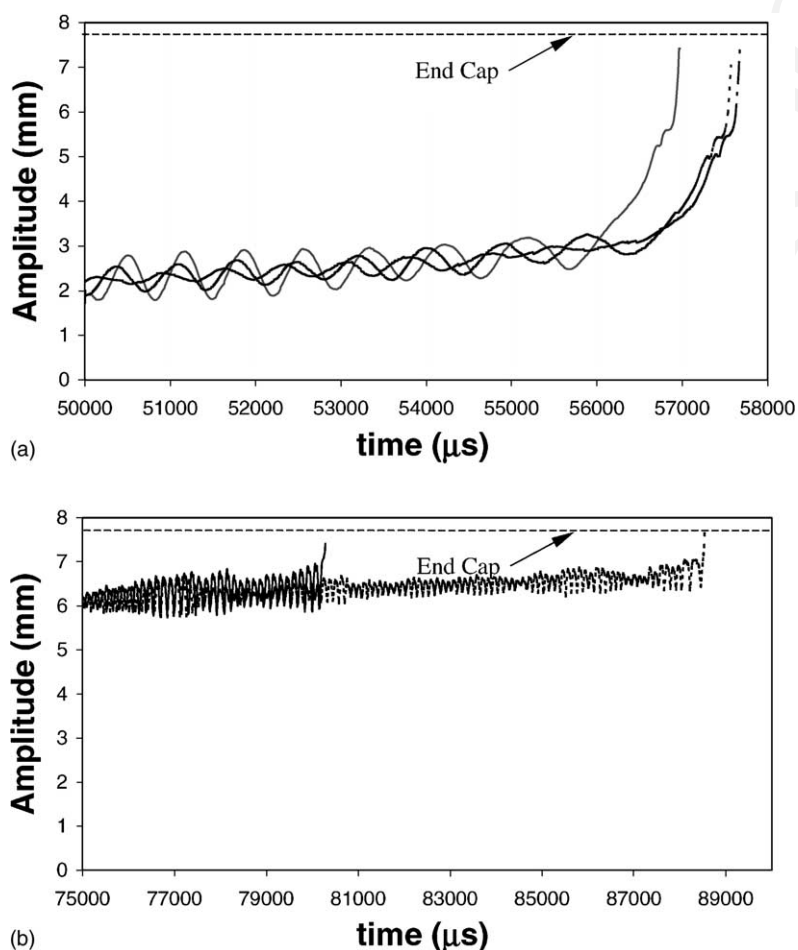


Fig. 7. Amplitude evolutions during a resonance ejection scan with a 10% stretched ion trap. The dipolar excitation is applied for  $q_z = 0.5$ , with width  $0.2T$ ;  $m = 3500$  Da,  $Z = 2$  for all ions. Buffer gas He pressure  $1 \times 10^{-3}$  mbar at 300 K. (a) Forward mass scan with  $V_{\text{dip}} = 50$  V; (b) reversed mass scan with  $V_{\text{dip}} = 10$  V.

the quadrupole electric field near the end-cap hole. Fig. 8 shows the arrangement of electrodes for this ion trap. Additional electrodes for the introduction of ions are also shown in the figure and are discussed later. The inner surface of the ion trap is pure hyperboloidal with the end-cap spacing  $2z_0 = \sqrt{2}r_0$ , corresponding to a pure quadrupole geometry. The exit end-cap hole is covered by a thin mesh to screen the negative field normally caused by the extraction electrode outside of the ion trap. The electric field generated by this electrode structure is basically a time variable quadrupole field with little higher-order multipole field compo-

nents. By applying an adjustable dc voltage  $V_{\text{fa}}$  to the field-adjusting electrode, the secular frequency shift prior to ejection can be adjusted to adequately (slight up shift, zero shift or slight down shift) to meet the analytical requirement.

Fig. 9a shows the evolution of the amplitudes of ion oscillation through the resonance ejection scan using the new ion trap. The voltage applied to the field-adjusting electrode is +1.5 kV and a 5 V,  $0.6T$  width pulsed dipolar excitation was used. The other parameters are the same as in simulation shown in Fig. 7a. In this case the expansion of ion oscillation

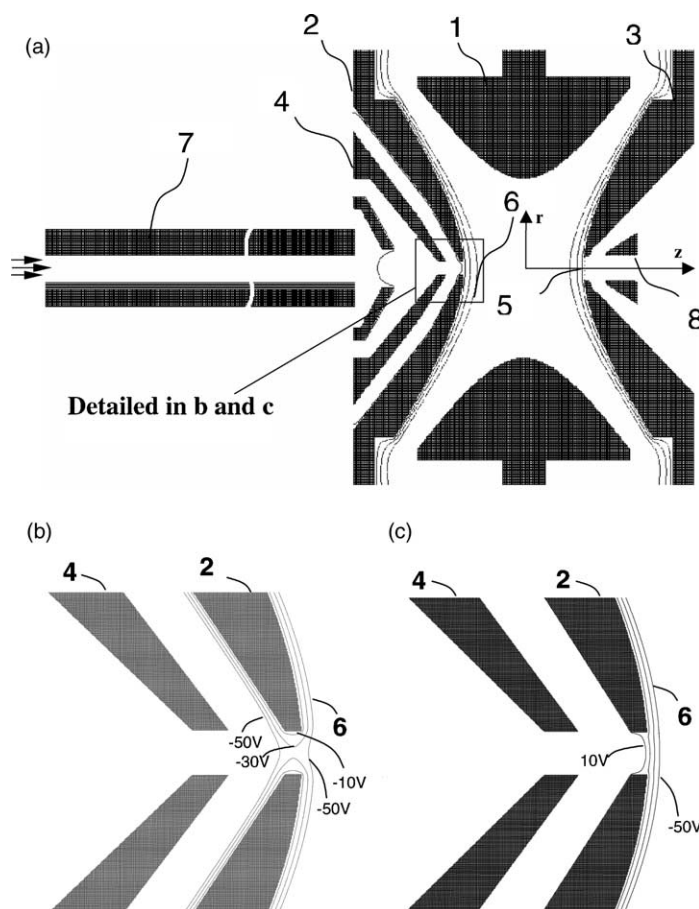


Fig. 8. A modified ion trap structure including 1, the ring electrode, 2 and 3, the end-cap electrodes; and 4, the field-adjusting electrode that was supplied with an adjustable dc voltage. Shown in the figure also: 5, the mesh used to cover the ejection end-cap hole; 7, octopole lens for ion introduction; and 8, the extraction electrode. The equipotential lines 6, of 10,  $-10$ , 30 and 50 V illustrated in the diagram (a) and detailed by diagram (c), are for the case when the ring electrode is charged at  $-1$  kV and the field-adjusting electrode is charged at  $+1.5$  kV. The same potential lines in the diagram (b) are for the case when the voltage on the field-adjusting electrode is changed to  $-400$  V.

is steadier and the ejection times for two sample ions are in good agreement.

By observing the ion motion, we can understand the mechanism behind the improvement. For resonance at a relative large  $\beta_z$  value (say  $\beta_z = 0.5$ ), an ion approaches the aperture only at the negative phase of the trapping field at which time the ring electrode is charged at  $-1$  kV. Referring to the Fig. 8a and c where the field-adjusting electrode four is applied with 1.5 kV dc voltage, the equipotential lines are not distorted near the apertures (in contrast, the field would be distorted as shown in Fig. 8b if the external electrode

near the end-cap is applied with a negative voltage  $V$  which is typically used for introduction of positive ions). In this case, an ion can maintain its oscillation frequency during the expansion until it hits the end-caps or is ejected through the aperture. Our ion motion simulation, in fact, shows a mild acceleration of ejection during the forward mass scan. This is explained by Fig. 10, where the ion is moving towards the resonance line of  $\beta_z = 0.5$ . When an ion approaches the end-cap, it sees an average dc field created by the field-adjusting electrode, that equates to an upward shift of the working point in the  $a$ - $q$  stability diagram

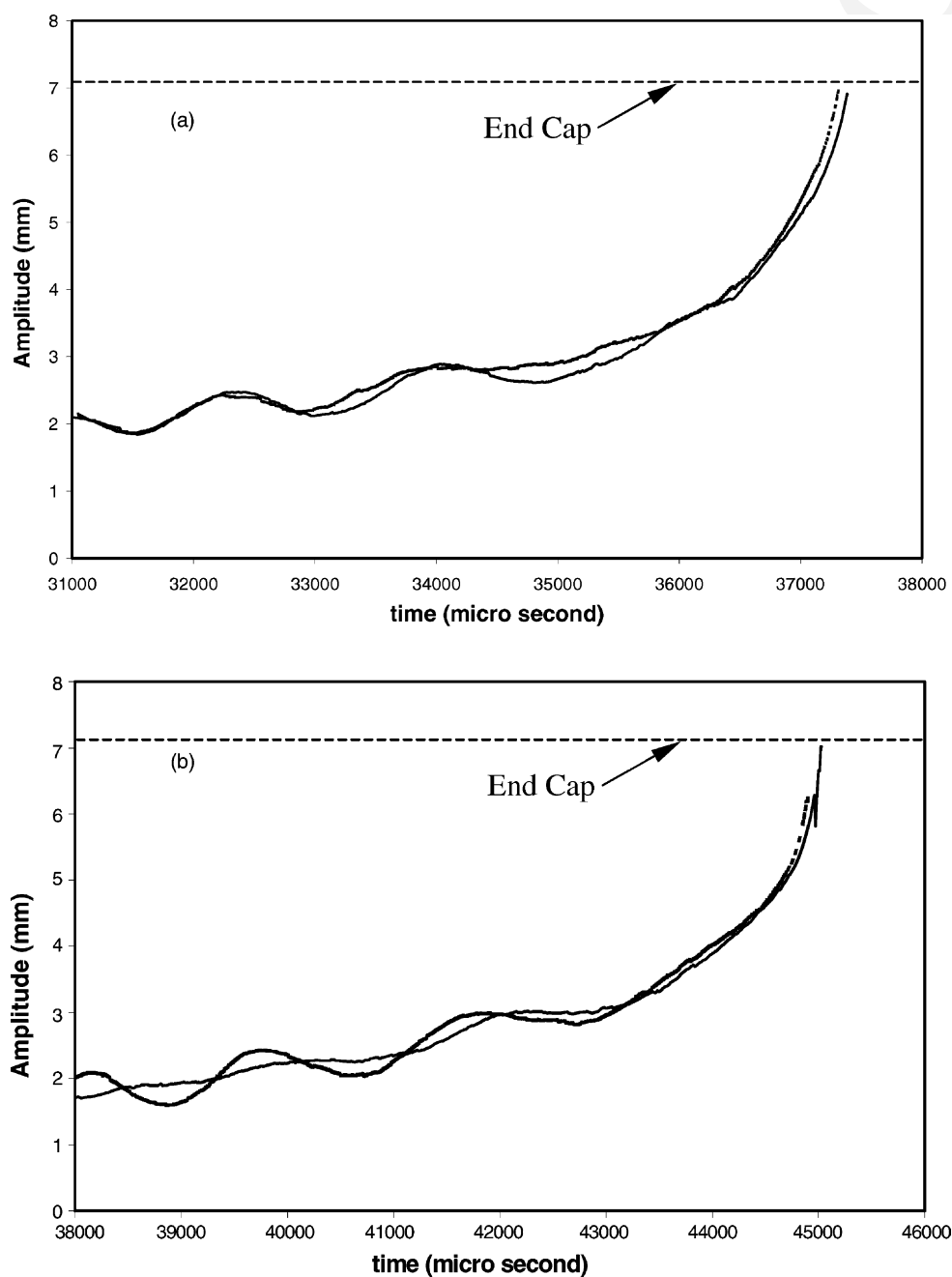


Fig. 9. Amplitude evolutions during a resonance ejection scan using the ion trap with a field-adjusting electrode. Rectangular drive voltage  $\pm 1000$  V, dipolar excitation at  $q_z = 0.5$  ( $\beta_z = 0.5$ ), with width  $0.6T$ ;  $m = 3500$  Da,  $Z = 2$ , buffer gas He pressure  $1 \times 10^{-3}$  mbar at 300 K. (a) Forward mass scan with  $V_{\text{dip}} = 5$  V,  $V_{\text{fa}} = 1.5$  kV; (b) reversed mass scan with  $V_{\text{dip}} = -4$  V and  $V_{\text{fa}} = 120$  V.

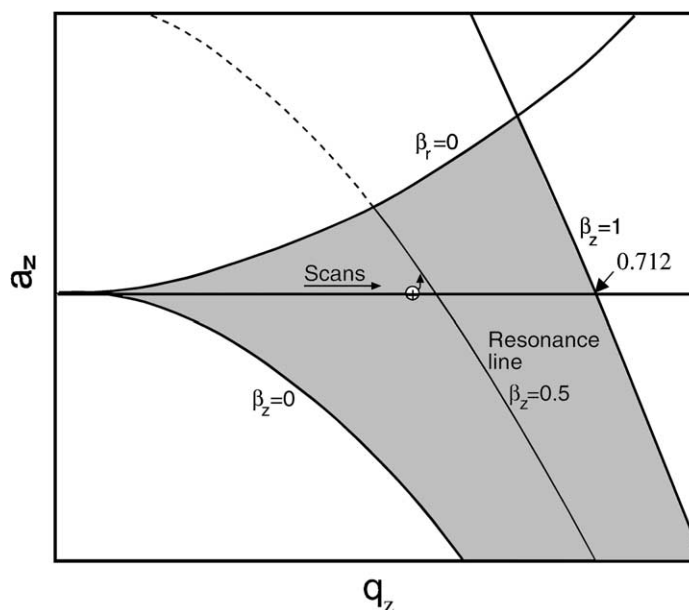


Fig. 10. The first stability region in which ions are scanned across the  $\beta_z = 0.5$  resonance line. An additional positive dc potential at the end-cap hole equates to an upward shift up in the  $a, q$  diagram for the ion which approaches to end-cap hole.

in Fig. 10. It is such a shift, that pushes an ion to enter resonance suddenly and causes the fast ejection.

Whilst applying a high positive voltage on the field-adjusting electrode enhances the performance of a forward mass scan, wherein the excitation frequency is matched by the secular frequency from the red side, the application of a relatively lower voltage (say 120 V for  $\pm 1$  kV driving voltage) on the field-adjusting electrode can accelerate ion ejection for a reverse mass scan wherein the excitation frequency is matched from the blue side. Fig. 9b shows the amplitude evolution through a reverse mass scan. Ion oscillation can expand steadily during the scan because the major part of the trapping region is subject to a pure quadrupole field. When an ion approaches the aperture, it experiences the negative higher-order multipole field because of insufficient positive compensation by the field-adjusting electrode. The negative higher-order field leads to a decrease of the secular frequency. In the case of a reverse mass scan, this red shift suddenly pushes the ion into resonance whereupon ejection occurs rapidly.

A high mass resolution reverse scan is useful for selecting precursor ions for tandem MS measurement. Here, a forward mass scan is carried out to eject all the ions having smaller mass/charge ratios than the selected precursor. A reverse scan is then imposed to eject the ions having higher mass/charge ratios than the selected precursor. The voltage on the field-adjusting electrode must be switched to the optimum value for each scan in order to obtain a clear clipping edge when these scans stop just before the mass/charge ratio of the precursor ion, and an ion cooling interval must be inserted in between the two scans. We expect that much smaller precursor selection window can be obtained by using this method in comparison with that obtained by normal notched wide band excitation method with a stretched ion trap where fixed higher-order field components permanently exist.

#### 4.5. Time of ejection and the mass resolution

In order to evaluate the mass resolution from the scan simulation, the statistics of ejection time for



Table 1

Achievable mass resolution  $R = M/\Delta M$  for different trap and scan speeds using same rectangular drive voltage of  $\pm 1$  kV and the resonance point of  $\beta_z = 0.5$ , simulated for mass 3500 Da and charge number 2

10% stretched ion trap	$R$	Field-adjustable ion trap	$R$
Forward 888 Th/s	4600	Forward 976 Th/s	13500
Forward 3550 Th/s	2500	Forward 3905 Th/s	6200
Reverse 1775 Th/s	320	Reverse 1953 Th/s	6000

The mean free path of ion in the He buffer gas is 15 mm.

multi- ions groups were used. Several groups, each of 20–60 ions, normally endured a scan through a range up to  $\Delta q_z = 0.01$ – $0.02$  (by varying  $T$ ), at scan speeds from hundreds to thousands Th/s. The flight time in these simulations is about 50 ms which is long enough to randomise the ion distribution under the buffer pressure of  $10^{-3}$  mbar. Mass resolution is calculated by assuming the ejection time has a Gaussian distribution, with a FWHM  $= 2.35\sigma_t$ , where  $\sigma_t$  is the standard deviation of the ejection time. Table 1

presents the results on the mass resolution for forward and reverse scan simulated with two types of ion trap.

Ejection time statistics showed the dependence of ejection time on the properties of the dipolar excitation waveform including the height  $V_d$ , the width  $w_d$  and the phase shift  $t_d$ , measured between the rising edge of the drive rectangular wave and the centre of the dipolar excitation pulse (refer to Fig. 1). The simulation was carried out with the field-adjustable ion trap and the resonance points were chosen as  $\beta_z = 0.5$  and  $0.667$ . In general, ions are ejected earlier when a higher  $V_d$  or  $w_d$  is used. If  $t_d$  is unchanged and the product of height and width is kept constant, the change in the averaged ejection time caused by the change in the ratio of width to height is less significant. For example, the change of ejection time for the variation of pulse height from 2 to 12 V, while the width from 0.6 to  $0.1T$ , respectively, is only from 38.15 to 38.9 ms, about twice the FWHM. However, the ejection time showed a strong dependence upon the phase shift  $t_d$ , even when  $V_d$  and  $w_d$  were kept constant. Fig. 11, using ejection

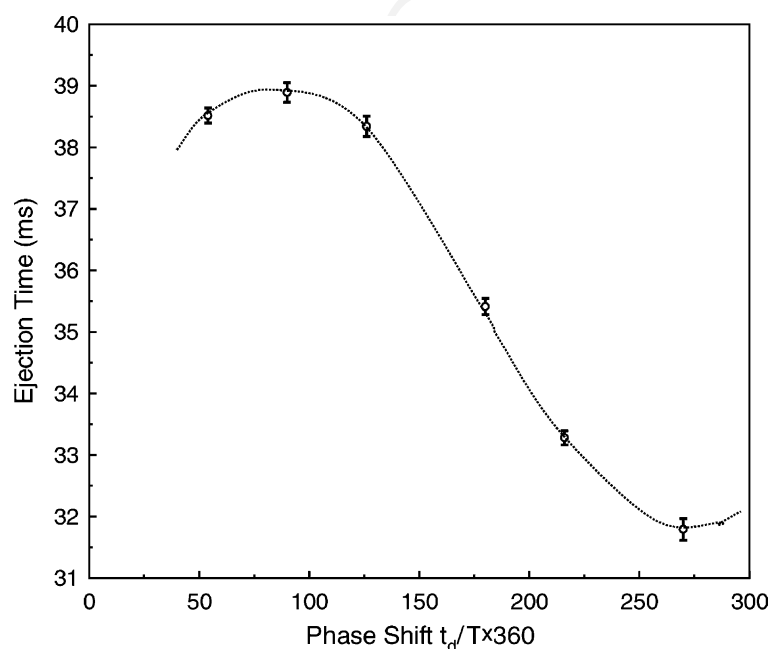


Fig. 11. The dependence of ion ejection time upon the phase delay measured between the centre of the dipolar excitation pulse and the rising edge of the drive rectangular waveform. The error bars show the FWHM of each ejection condition.

time statistics, shows such a dependence. Ejection of all groups was accomplished with a  $4\text{ V} \times 0.3T$  dipolar excitation. The shortest time for ion ejection occurs when the centre of the dipole pulse was located in the middle of the negative excursion of the drive voltage, and longest when it moves to the middle of the positive excursion. For a comparison, error bars are used in this figure showing FWHM for each group of ejection. The whole span of ejection time caused by the phase shift is more than 20 times larger than an averaged FWHM. This observation indicates that mass resolution could be considerably impaired when the dipolar excitation pulse is applied without phase locking it to the drive rectangular voltage. A similar simulation study that employed an analogue ion trap has been reported by Londry and March [21], who suggested that phase locking between the drive rf and the dipolar tickle voltage, both being sinusoidal waveform voltages, improved the mass resolution. In the DIT where the dipole excitation pulse is derived from the same timing controller as the driving rectangular wave, the phase relation is kept constant and can be optimised by the software so that the highest mass resolution is guaranteed.

#### 4.6. Space charge effects

Space charge causes many problems in ion trap operation and not all of them can be studied easily by simulation. The multi-ion simulation capability of SIMION 7 allows the charge repulsion to be considered during the ion motion simulation. In order to have sufficient repulsion, or in other words to see the space charge effect, we took SIMION 7's factor repulsion method, where each ion represents several ions of the same mass/charge ratio and the total influence is applied to the other ions. In our simulation, when we ran  $n$  groups of 20 ions and set the factor 50, ions behaved as though there was an ion cloud of  $n \times 1000$  ions and a space charge effect was exhibited.

Fig. 12 uses the ejection time data from grouped ion simulations and is presented in the form of the number of ejections in each  $50\text{ }\mu\text{s}$  interval to show the mass peak distributions. In each simulation the mass/charge ratios of the groups were 3499/2, 3500/2 and 3501/2, and each group had 20 ions. The plots in Fig. 12 show different factors by which each ion was multiplied to represent a multiple of ions. The first plot is for no repulsion. Upon a factor of 10, which translates to 600

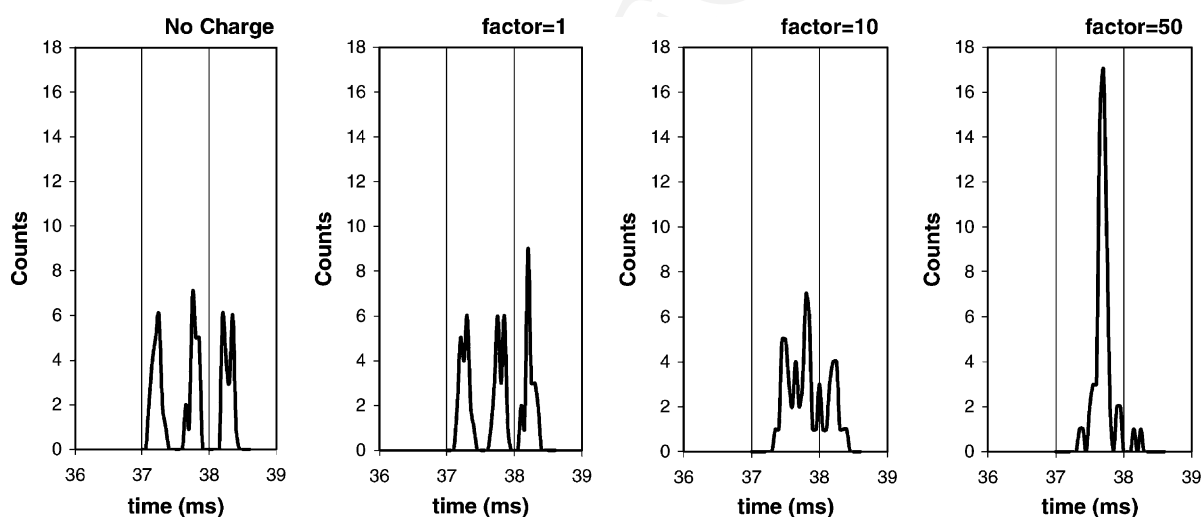


Fig. 12. The ejection time distribution for three ejected ion groups having masses of 3499, 3500, 3501 and charge  $2e$ , and its change due to the space charge influence. The first plot takes no account for ion repulsion but the following plots show repulsion for total ion numbers of 60, 600 and 3000, respectively.

ions within a 1.5 Th mass range, space charge already causes the mass peaks to coalesce. At a factor of 50 (3000 ions within the same narrow mass range) all ions are ejected in one group. Although the statistical resolution from the FWHM may be even better, the masses are practically unresolved.

#### 4.7. Quadrupole excitation by duty cycle modulation

Parametric resonance in the quadrupole ion trap can be utilised for quadrupolar excitation and it does not require that the dipolar tickle voltage be applied to

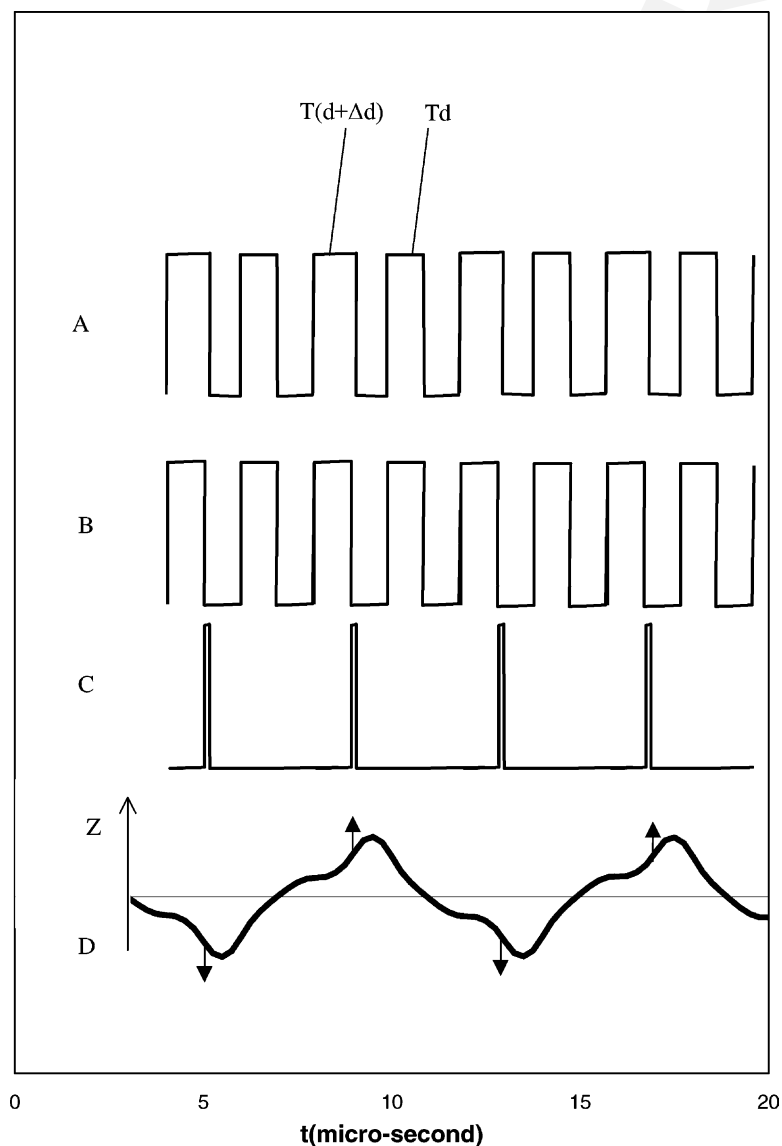


Fig. 13. Quadrupolar resonance excitation achieved by duty cycle modulation of the drive rectangular waveform. A, drive waveform with every other duty cycle increased by  $\Delta d$ . A can be decomposed to B, an equal duty square wave and C, a narrow pulse effectively excites the ion motion shown in D.

the end-caps. One of the advantages of DIT is that quadrupolar excitation can be easily implemented by modifying the digital control timing. Fig. 13 illustrates a method whereby the duty cycle of the rectangular drive waveform is modulated to excite the ions in the  $z$  direction. In fact, the modulated waveform A can be decomposed into a non-modulated waveform B and a narrow excitation pulse C. At resonance, the narrow excitation pulses keep pushing an ion in the direction of its motion, and this push will keep in phase with the double frequency of the secular motion. It can be shown that resonance excitation at  $\beta_z = m/n$  may be achieved when every  $n$ th wave is modulated, where  $m$  is an integer.

In the DIT, the addition of a small delay to the selected falling edge produces duty cycle modulation. This modulation can be used for a resonance ejection mass scan similar to that with dipolar excitation. Fig. 14 shows the evolution of trajectory amplitude

during such a resonance ejection scan. The simulation was carried out with a field-adjustable ion trap and the amount of modulation was 5% of the drive period  $T$ . Even with 0.5%  $T$  modulation, the excitation power is still sufficient to eject the ions. Because of the nature of quadrupolar excitation (excitation force  $\propto$  distance from the centre), the ejection speed is very fast. However, the two curves for ions of the same mass/charge ratio shown in Fig. 14 do not come together at the point of ejection and the statistics give a mass resolution of  $<2000$  for such a scan. The strong and randomly-phased beat shown in Fig. 14, although having nothing to do with the higher-order multipole field, causes the dispersion of the ejection time.

#### 4.8. Ion injection to DIT

In principle, ions generated outside a quadrupole ion trap cannot be trapped when the ion trap is driven

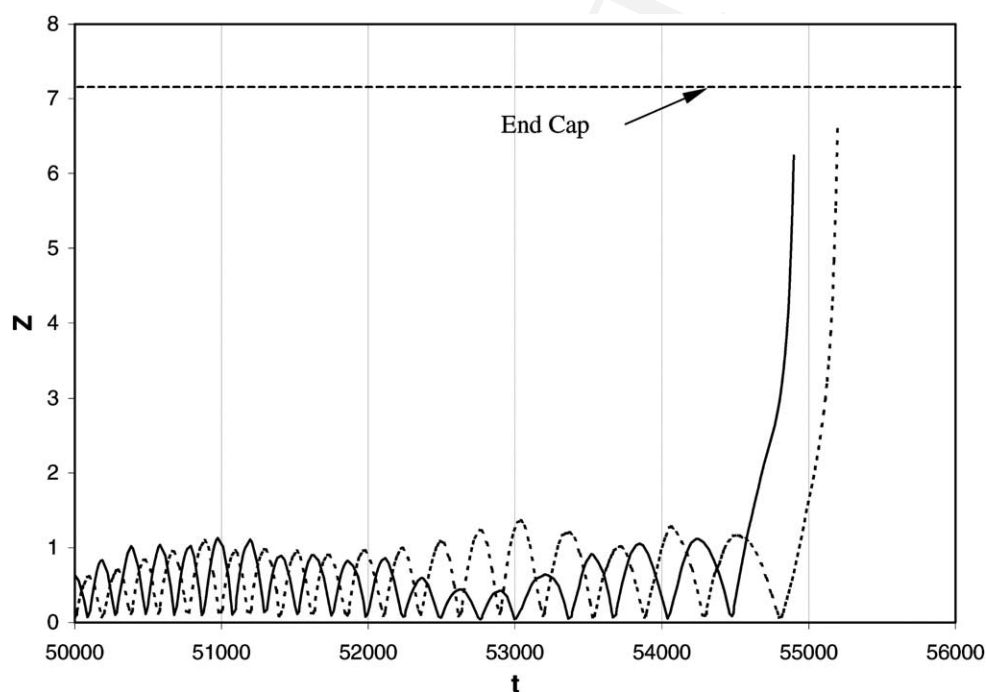


Fig. 14. The evolutions of the trajectory amplitudes for two ions, both  $m = 3500$  and  $Z = 2$ , during a mass scan using resonance ejection by duty cycle modulation. Refer to Fig. 13,  $\Delta d = 5\%$  at every other wave, rectangular drive voltage  $\pm 1000$  V,  $V_{fa} = 1.6$  kV and buffer gas He  $1 \times 10^{-3}$  mbar, 300 K.

by a fixed, periodically changed ac voltage, no matter whether the driving voltage is analogue or digital. This is due to the energy of the ion upon entry to the trapping volume being always higher than the pseudo-potential well depth. Damping gas, normally helium or nitrogen, is used in modern ion trap technology to reduce the kinetic energy of the injected ions providing a mechanism whereby ions may be trapped. Simulation of such a trapping process is also important for DIT operation.

Depicted partly in Fig. 8, the geometry for the simulation includes an octopole ion guide, two static lenses one of them being the field-adjusting electrode, and the DIT. The flight of ions in each section is simulated by a separate user program, which includes modelling ion elastic collisions with a buffer gas. Ions are fired continuously from the one end of the octopole with Gaussian spatial and energy distributions having standard deviations of 0.2 mm and 0.1 eV, respectively. They are first accelerated to 10 eV and drift through the octopole where the buffer gas species and pressure are changed gradually along the axis from 0.02 mbar of N<sub>2</sub> to 0.03 mbar of He at the ion trap. Such an introduction system is commonly used for coupling an ion trap to an electrospray ion source or a chemical ionisation source. The applied voltages

are: octopole:  $V_{rf} = 200$  V, 1.2 MHz plus a certain dc bias; first static lens,  $-10$  V; field-adjusting electrode,  $-50$  to  $800$  V; end-caps,  $0$  V and the DIT operates with a  $\pm 1$  kV square wave.

Ions that survive 500 rectangular wave periods in the ion trap are regarded as being permanently trapped. Statistical examination of simulated trajectories showed that ions can enter the ion trap only in the negative excursion and centred about  $0.8T$  from the rising edge, otherwise they are rejected back into the octopole section. Fig. 15 shows the mass/charge ratio dependence of the trapping efficiency for a DIT driven by a  $T = 3 \mu\text{s}$  waveform. After the low mass cut-off, there are several maxima at masses of 1800, 2300, 2550 Da, etc. These maxima appear because the secular motion returns an ion back to the entrance at the ‘good phase’ of the drive field (also in the negative excursion). At such a phase, ions will be rejected back into the trapping volume and may be trapped with higher efficiency. The next maximum appears at a higher mass of the ion which returns to the entrance at the ‘good phase’ of the next drive rectangular voltage.

The above phenomenon clearly exists for trapping of the ions with higher  $q_z$  ( $>0.2$ ), in which case an ion’s secular motion has a higher frequency and is harshly interfered with a higher harmonic component. In

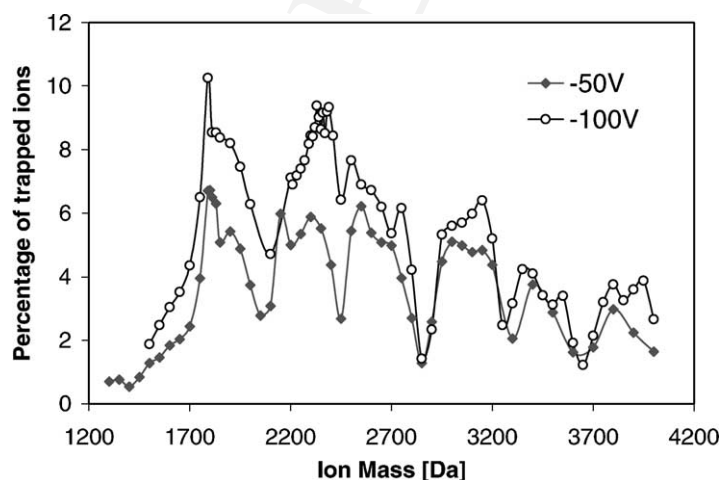


Fig. 15. Trapping efficiency for ions of various mass/charge ratio and generated outside of the ion trap. The theoretical low mass cut-off is 1229 Th. The voltage of the field-adjusting electrode is  $-50$  and  $100$  V for the two sets of data.

practice, the introduction with a high  $q_z$  value often suffers ion loss by collision induced fragmentation because the velocity of the ion is high. This has been evidenced in an experiment with a conventional analogue ion trap [22]. For lower  $q_z$  values (higher mass/charge ratio and drive frequency) ions trajectories are close to a harmonic oscillation with very little driving frequency ripple. The mass dependence of the trapping efficiency becomes less significant. Where fragmentation loss is reduced, the collisional cooling is less effective also, so the heavy ions can easily escape from the ion trap with their undamped initial energy. Nevertheless ions need sufficient initial energy to enter the ion trap without suffering large perturbations at the entrance. Using the field-adjusting electrode at the entrance aperture and applying sufficient negative voltage to it, the potential well may be modified to look like a bowl with a narrow ‘notch’ on its edge (refer to Fig. 8b). Ions even with an initial energy lower than the edge of the potential well (negative energy) can get into the well through the ‘notch.’ These ions cannot hit the ion trap electrodes

nor escape from the trap unless they return to the entrance point where the notch is. When a radial velocity exists, it takes a relatively long time for the ions to find this notch and escape, increasing the probability of cooling and subsequent entrapment.

Fig. 16 shows the trapping efficiency in case. Ions start with an initial kinetic energy of 15 eV while the potential of the starting point is  $-20$  V with respect to the grounded entrance end-cap. The mass is 6000 Da and the  $T = 2 \mu\text{s}$ . When the voltage of the field-adjusting electrode is  $-450$  V, the efficiency reaches the maximal value of 8.4%.

With a symmetric square wave drive voltage, where  $a = 0$ , the secular frequency in two directions has the approximate relation  $\omega_r = 1/2\omega_z$ . The ion, after its first secular cycle in the  $z$  direction will return to  $z = z_0$ ,  $r = 0$ , where the entrance ‘notch’ mentioned above locates. When the mass range of trapping is not a priority, a specific dc component to the trapping field can be used, producing  $a \neq 0$ . In such a case, the secular frequency in the  $r$  direction can be distant from the half frequency of that in the  $z$  direction

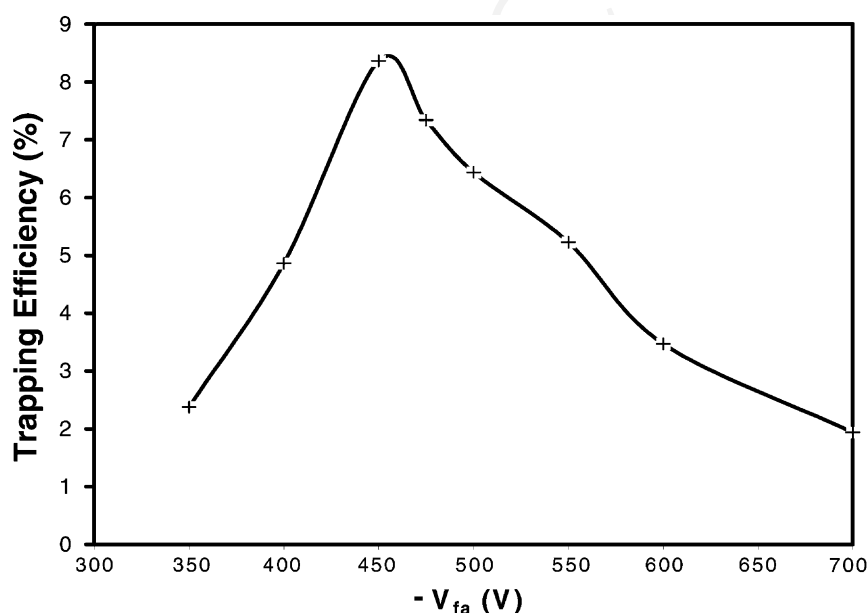


Fig. 16. The dependence of trapping efficiency upon the potential applied to the field-adjusting electrode. Singly charged ions of mass 6000 Da and initial kinetic energy 15 eV start from an electric potential of  $-20$  eV relative to the end-cap electrode. The mean free path in the ion trap is set to be 5 mm.



so it is harder for ions to return to the ‘notch’ and escape.

Ions introduced from a pulsed ion source are well suited to the DIT. The trapping rectangular wave can be stopped until the ions enters the trapping volume and it can switched on from the desired optimum phase (say around  $0.75T$ ). The dipole pulse can help to damp the initial energy during the introduction. A high efficiency of trapping can be predicted based on previous work [14,23]. While it would be interesting to see the simulations of such an operation with a DIT, it is not within the scope of the current paper.

At the review stage of current paper, a research by Appelhans and Dahl on ion injection for the ion trap mass spectrometer was published [24]. In there, the simulations were able to be compared against the results from well designed experiments, although the ion trap was not driven digitally in either the simulation or the experiment. The modelling of ion buffer collision in their work is similar to ours except that the buffer particle’s velocity has not been considered in their program. The interesting agreement between their experiments and simulations encourages us to pursue further an experimental study on the DIT.

## 5. Conclusion

A sophisticated user program used in conjunction with SIMION has been employed for a study of DIT operation. Modelling three-dimensional ion buffer gas collisions, with the relative velocity of the collision partners taken into account, made it possible to show various processes in the ion trap such as ion cooling, ion heating and maintenance of equilibrium.

A mass-selective ejection scan method is described and simulated, where both the trapping quadrupole field and the dipolar excitation field are driven in a digital manner and their frequencies are scanned proportionally. The simulations show that the commercially available stretched ion trap effects fast ion ejection, but the associated strong beat in ion oscillations impair mass resolution.

Correction of the field at the end-cap hole is achieved by using a field-adjusting electrode near the end-cap aperture. The resultant new ion trap geometry has been shown by these simulations to have high mass resolution (up to 13,500) for both forward mass scans and reverse mass scans. Such an ion trap, with its two-step scan, can be used for high mass resolution precursor selection. It can also be expected, by comparing the high resolution mass spectra scanned in opposite directions, that real chemical shifts due to the structural difference of ions can be identified.

Duty cycle modulation of the drive rectangular waveform can be an alternative method for executing a mass-selective ejection scan, and such modulation removes the necessity of applying the dipolar excitation voltage to the end-caps.

Other important results obtained from these simulations, include the ejection time dependence on the phase of pulsed dipolar excitation, the influence of space charge, and the behaviour of ions injected into the ion trap. The space charge simulation applies only to the situation where all of the ions have mass/charge ratios in a small range; however, the software used is also capable of simulating other practical situations.

It is worth mentioning that using a dc voltage to adjust the field at the end-cap aperture to achieve enhanced performance can also apply to the quadrupole ion trap driven by a conventional harmonic rf power supply. However, as some unique features of DIT have been demonstrated in this simulation study, we believe that DIT technology will extend the applications of ion traps in the future.

## Uncited reference

[2].

## Acknowledgements

Li Ding thanks Prof. E.P. Sheretov for discussions on some related topics. Michael Sudakov wishes to thank Dr. D. Dahl for the discussion on the application of Monte Carlo simulations in SIMION 7. We thank

Mike May for his help in proof reading this document and the reviewers for their careful and thoughtful critique. Finally, we express our thanks to Shimadzu Corp. in Japan for the funding of this project.

## References

- [1] W. Paul, H. Steinwedel, US Patent 2,939,952 (1960).
- [2] R.E. March, J.F.J. Todd (Eds.), *Practical Aspect of Ion Trap Mass Spectrometry*, vol. 1, CRC Press, Boca Raton, FL, 1995.
- [3] G.C. Stafford, P.E. Kelley, D.R. Stephens, US Patent 4,540,884 (1985).
- [4] J.E. Fulford, D.-N. Hoa, R.J. Hughes, R.E. March, R.F. Bonner, G.J. Wong, *J. Vac. Sci. Technol.* 17 (4) (1980).
- [5] R.E. March, R.J. Hughes, *Quadrupole Storage Mass Spectrometry*, Wiley Interscience, New York, 1989.
- [6] B. Landais, C. Beaugrand, L. Capron-Dukan, M. Sablier, G. Simonneau, C. Rolando, *Rapid Commun. Mass Spectrom.* 12 (1998) 302.
- [7] U.P. Schlunegger, M. Stoeckli, R.M. Caprioli, *Rapid Commun. Mass Spectrom.* 13 (1999) 1792.
- [8] E.P. Sheretov, Z.V.I. Terent'ev, *Tech. Fiz.* 42 (5) (1972) 953.
- [9] E.P. Sheretov, V. Gurov, M. Safonov, I. Philippov, *Int. J. Mass Spectrom.* 189 (1999) 9.
- [10] A. Richards, M. Huey, J. Hiller, *Int. J. Mass Spectrom. Ion Phys.* 12 (1973) 317.
- [11] L. Ding, S. Kumashiro, *Chin. Vacuum Sci. Tech.* 21 (3) (2001).
- [12] L. Ding, A. Gelsthorpe, J. Nuttall, S. Kumashiro, *Rectangular wave quadrupole field and digital Q(IT)MS technology*, in: *Proceedings of the 49th ASMS Conference, MPC80, Chicago, 2001*.
- [13] N.V. Konenkov, M. Sudakov, D.J. Douglas, *J. Am. Soc. Mass Spectrom.* 13 (2002) 597.
- [14] L. Ding, E. Kawatoh, K. Tanaka, A.J. Smith, S. Kumashiro, *Proc. SPIE Charged Particle Opt. IV V3777* (1999) 144.
- [15] R. Julian, M. Nappi, C. Weil, R.G. Cooks, *J. Am. Soc. Mass Spectrom.* 6 (1995) 57.
- [16] R.M. Waldren, J.F.J. Todd, in: D. Price, J.F.J. Todd (Eds.), *Dynamic Mass Spectrometry*, vol. 5, Heyden, London, 1978, p. 14.
- [17] M.W. Forbes, M. Sharif, T. Croley, Z. Lausevic, R.E. March, *J. Mass Spectrom.* 34 (1999) 1219.
- [18] Y.-L. Chen, B.A. Collings, D.J. Douglas, *J. Am. Soc. Mass Spectrom.* 8 (1997) 681.
- [19] J. Franzen, R.-H. Gabling, M. Schubert, Y. Wang, in: R.E. March, J.F.J. Todd (Eds.), *Practical Aspects of Ion Trap Mass Spectrometry*, vol. 1, CRC Press, Boca Raton, FL, 1995, p. 49.
- [20] M. Wells, W. Plass, R.G. Cooks, *Anal. Chem.* 72 (13) (2000) 2677.
- [21] F.A. Londry, R.E. March, *Int. J. Mass Spectrom. Ion Process.* 144 (1995) 87.
- [22] S.T. Quarmby, R.A. Yost, *Int. J. Mass Spectrom.* 190/191 (1999) 81.
- [23] P. Kofel, in: R.E. March, J.F.J. Todd (Eds.), *Practical Aspect of Ion Trap Mass Spectrometry*, vol. 2, CRC Press, Boca Raton, FL, 1995, p. 51.
- [24] A.D. Appelhans, D.A. Dahl, *Int. J. Mass Spectrom.* 216 (2002) 269.